Application of Coupled Oscillator Model to Terahertz and Optical Control of Plasmon Induced Opacity in Coupled Metamaterials

Submitted to the Department of Physics
Oregon State University

In partial fulfillment of the requirements
for the degree of B.S. in Physics

Milo X. Sprague

Submitted on
05/04/2021

Table of Contents:

Table of Figures:

Application of Coupled Oscillator Model to Terahertz and Optical Control of Plasmon Induced Opacity in Coupled Metamaterials

Abstract

Terahertz (THz) frequencies of the electromagnetic spectrum have been underutilized when compared to neighboring microwave and infrared frequencies, largely due to the difficulties controlling and detecting these fields. In a step toward gaining control over THz frequencies, my advisor Dr. Yun-Shik Lee's group experimentally demonstrated optical-pulse THz-control over a plasmonic metamaterial. To complement the experiments, I theoretically model the system using a coupled linear oscillator model to describe plasmonic oscillations of the metamaterial. The parameters of this oscillator model are fitted to the THz-Time domain spectroscopy results from the experimental counterpart without the presence of an optical pulse. Enhanced control of the THz response was experimentally demonstrated by the group by optically exciting charge carriers in a GaAs substrate, which was found to interfere with the plasmon-induced opacity in a predictable manner. Furthermore, these experiments show that plasmon-induced opacity can be reintroduced in the photoconductive sample by increasing incident THz field strength. These observations are modelled theoretically by introducing time dependence to the damping rates of the coupled linear oscillator model. The relation between the oscillator damping rates and THz field strength is attributed to phonon-assisted intervalley tunneling in large THz fields, which involves a decrease in substrate conductivity as electrons tunnel to side valleys with larger effective mass. A simple description of intervalley scattering is done using a two state population model where only electrons in the lower-energy Γ-valley state contribute to substrate conductivity. The final results of my model replicate the THz response of the composite metamaterial sample with and without optical excitation, as well for differing THz field strengths. We observe the oscillation of THz transmission through the sample over sub-picosecond shifts in the optical pulse delay time, which is a consequence of intervalley scattering induced by plasmonic oscillations in the metamaterial. Finally, the size and temporal locations of these modulations in transmission are shown to be intimately related with transport properties of the substrate, such as intervalley scattering rates and mean-free times.

I. Introduction

I. 1. Motivation

The terahertz (THz) region of the electromagnetic spectrum, situated between microwave and infrared frequencies, represents an underutilized tool in optical science and engineering[1]. Currently THz radiation is applied as a probe for baggage security, micron-scaled electron device imaging, and for the study of many-body interactions in condensed matter physics, among other applications. However, unlike the heavily utilized microwave and infrared frequencies, the technical difficulties associated with the generation, manipulation, and detection of THz waves have prevented their full practicalization. Metamaterials could supply the necessary control over THz waves that would allow for increased applicability in science and industry. Since metamaterials are engineered devices, their dimensions and layouts can be designed to interact with THz fields to produce an intended diffraction effect. Here we theoretically model the THz response of an example composite metal-semiconductor metamaterial. The plasmonic oscillations within the metamaterial are described as coupled linear oscillators, where changes to substrate conductivity are accounted for by changing oscillator damping rates.

The purpose of this project is to apply the coupled oscillator model to the problem of THz control. The capacity of the model to describe THz and optical responses of a metamaterial is judged by its ability to replicate experimental optical pump - THz control time domain spectroscopy measurements of a plasmonic metamaterial obtained in the lab of Dr. Yun-Shik Lee at Oregon State University. The metamaterial sample used by the experiment sister-project is designed to have an opaque gap in its spectrum at a certain resonance frequency. Changes to this plasmon-induced opacity (PIO) signature by THz and optical pulses incident on the metamaterial serve to test accuracy of the oscillator model.

I. 2. Plasmon Induced Opacity in Metamaterials

The optical properties of natural materials are defined by the polarizability of constituent atoms and molecules in response to incident electromagnetic radiation. Internal polarization of the material causes new electromagnetic waves to be produced by the oscillation of bound charges, which interfere with the incident wave to produce refraction, reflection, transmission, absorption, etc. It follows that fabricating an artificial material, or metamaterial, with a geometry to polarize charges and currents in ways uncommon in naturally occurring substances could unlock a range of new optical phenomena.

Plasmonic metamaterials are a subclass of metamaterials that utilize the generation and interference of plasmonic responses. Plasmonic oscillations consist of the coupling of free electrons within a conductor to a propagating electromagnetic field. A stable unattenuated propagation of a plasmonic oscillation along a metallic surface is achieved when surface currents are able to compensate for the displacement current term in Ampere's law. A plasmonic metamaterial uses the presence of resonating surface current modes to selectively respond to certain incident electromagnetic fields.

Plasmon induced opacity (PIO) is one application of plasmonic metamaterials, where the transmission of electromagnetic fields within a narrow frequency band diminishes considerably. This works by having a lattice of two types of resonators polarized in different ways. These resonators, through their mutual capacitance and inductance, couple to one another producing the interference effect. The pertinent metamaterial in this study consists of a linear dipole antenna situated in between a pair of split ring resonators (SRRs) cut from an aluminum film (*Figure I-1)*.

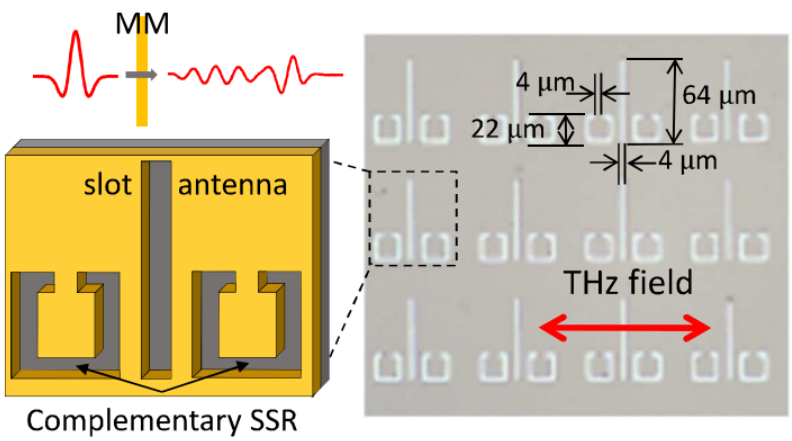

Figure I-1. Diagram and microscope image of the metamaterial surface[2]. The resonators within a unit cell are cut from an aluminum sheet of thickness $0.5\mu m$. The dipole resonator is a rectangular slot resonator with dimensions $64\ \mu m$ by $4\ \mu m$. The dipole resonator is situated between two split ring resonators with dimensions indicated.

The linear dipole resonator allows the surface currents perpendicular to the slit to couple to transmitted electromagnetic fields passing through the gap. This coupling of surface currents and EM fields along the surface produces a *plasmonic oscillation.* The presence of these surface plasmons determines the ability of the dipole resonator to transmit THz fields. The dipole resonator plays the role of the radiative or "bright" element, as it strongly couples to external electromagnetic radiation.

Immediately adjacent to the dipole resonator are a pair of *split ring resonators* (SRRs). The geometry of the split ring resonators does not adequately support the coupling of surface currents to EM radiation that produce plasmonic oscillations. The SRRs thus play the role of the subradiant, or "dark" element in the metamaterial. Due to the close proximity of the dipole resonator and the SRR pairs, surface currents and charge accumulations in one element couple through mutual inductance and capacitance with the other.

Radiative damping of the dipole resonator broadens the electric susceptibility around its resonance frequency, whereas the lower damping rate of the SRRs produces a sharper resonance within a narrow frequency range. The spectral response by the coupled metamaterial system then is dominated by the dipole bright mode away from the dark mode

resonance frequency. Incident THz frequencies near the SRR dark mode resonance are not transmitted due to the destructive interference between the bright and dark modes (*Figure 2*).

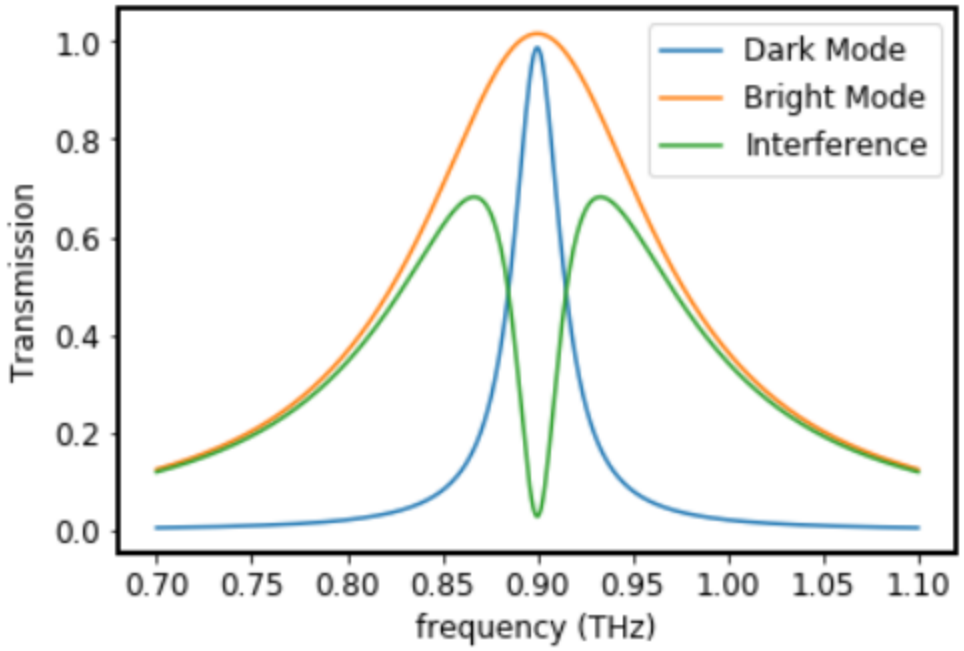

Figure I-2. Example sketch of PIO interference effect. Bright mode (yellow) is a Lorentzian function broadened by high radiative damping. Dark mode (blue) is given by a narrow Lorentian curve. The PIO interference effect (green) is qualitatively given as the difference between the bright and dark mode susceptibilities.

Additional damping is introduced by the finite conductivity of the resonant cavity walls. Propagating modes within the resonators are attenuated when plasmonic oscillations are not able to instantaneously respond to incident fields [3]. Increased conductivity in the GaAs substrate is an additional source of attenuation[4,5].

I. 3. Optical and THz Substrate Damping

The substrate on which metamaterial is implanted can also influence the plasmonic oscillations. Here we use the intrinsic semiconductor GaAs as the substrate material. Intrinsic GaAs is a dielectric material and thus can influence the metamaterial resonance frequencies through capacitance increases. Optical excitation of the GaAs however produces a conductive substrate, which can "short circuit" the gaps of the metamaterial resonators. The result is highly damped plasmonic oscillations as they couple to substrate currents. This optical damping effect strongly inhibits the PIO effect observed in the unexcited sample.

Substrate currents are generated from the response of conducting electrons and holes in the GaAs crystal. Incident photons with energy higher than the band gap (~1.4 eV in GaAs) can generate electron-hole pairs. Carrier transport is dominated by conduction electrons, as holes have relatively low mobility in GaAs.

Conduction electrons with low kinetic energy occupy the Γ-valley (*Figure I-3*), where transport properties are described by a quasiparticle with the electron's charge e and a mass $m_{\Gamma}^{*} \approx 0.067\, m_e$, where m_e is the mass of the free electron. Due to the band structure of GaAs, conduction electrons with sufficient kinetic energy can scatter into several *side valleys*. Electrons within these side valleys have a much higher effective mass, which decreases their mobility in response to external electromagnetic fields.

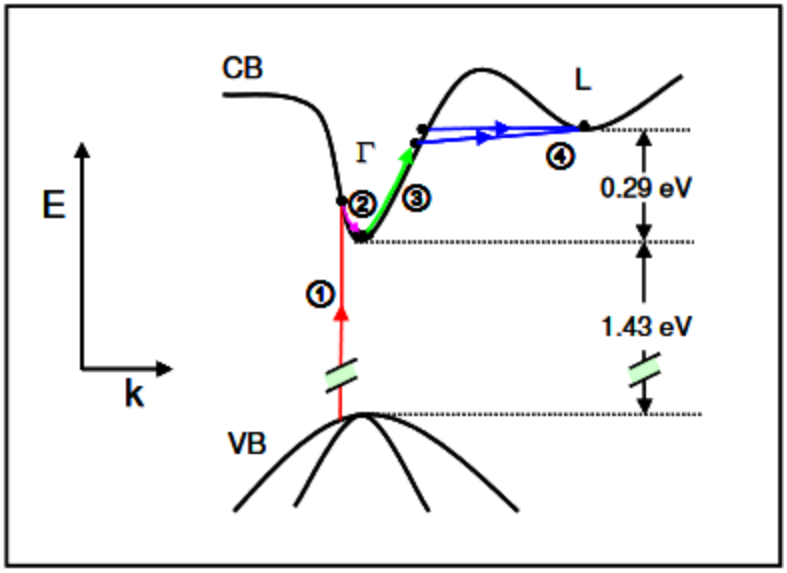

Figure I-3. High energy conduction electron dynamics within the GaAs band diagram from FH Su, et.al.[6] Step (1) depicts the optical excitation of electrons from the valence band (VB) to the conduction band (CB). (2) shows the fast relaxation of electrons into the bottom of the Γ valley. (3) depicts electrons being driven by an external electric field before (4) tunneling into the adjacent L valley.

The properties of the GaAs conduction band can be practically utilized by combining optical and THz pulses to facilitate the conduction band processes labelled in *Figure 3.* An optical pulse with wavelength shorter than about 870 nm, or energy greater than 1.4 eV, is capable of photoexciting electrons from the valence band to the conduction band (step (1) in *Fig 3.*). THz fields are able to increase the kinetic energy of Γ valley electrons (step (2)). Once these electrons are sufficiently energetic, optical phonon scattering facilitates the intervalley tunneling of electrons from the Γ valley into the L valley.

It is apparent now that the detailed band structure of GaAs becomes important when THz fields of various strengths are involved. Carrier dynamics are dominated by the mobile Γ valley electrons, therefore modelling the Γ valley population is key to deriving the currents J in the GaAs substrate (eq. I-1).

$$J \approx e n_{\Gamma} v \tag{I-1}$$

Where e is the electron charge and v is the Γ valley electron's acquired velocity.

II. Methods

II.1. Coupled Linear Oscillator Model

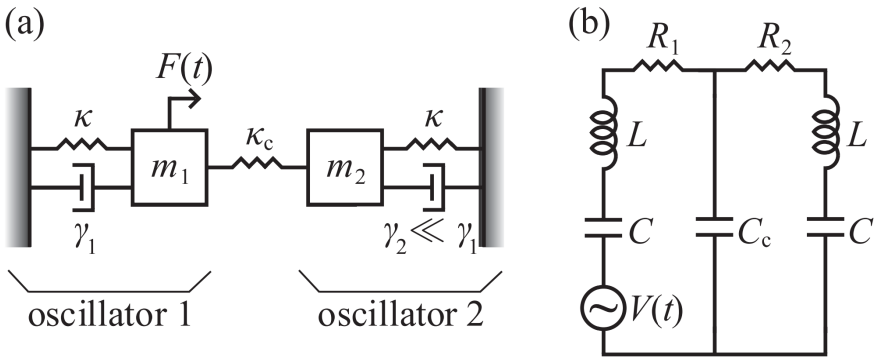

Figure II-1. Two examples of mathematically equivalent coupled harmonic oscillator systems[7]. Both the mechanical system (a) and the electronic system (b) consist of a driving force/voltage, respectively, acting on one of the two oscillators.

A pair of coupled harmonic oscillators can be shown to exhibit the induced opacity effect we see in plasmonic metamaterials. Since the component resonators comprising the metamaterial are inductively and capacitively coupled, it's reasonable to model the system as an LC circuit described by the behavior of coupled linear oscillations[7].

$$\begin{aligned} \ddot{q}_1 + \beta_1 \dot{q}_1 + \omega_{r;1}^2 q_1 + \omega_c^2 q_2 &= Q f(t) \\ \ddot{q}_2 + \beta_2 \dot{q}_2 + \omega_{r;2}^2 q_2 + \omega_c^2 q_1 &= 0. \end{aligned} \tag{II.1}$$

The first oscillator q_1 is being driven by the incident electromagnetic waves *f(t)* through the dipole coupling term Q. The oscillator modes have a damping factor β_1 and β_2 due to losses to surface currents. Each mode has a natural resonant frequency of $\omega_{r;1}$ and $\omega_{r;2}$. The oscillation magnitudes are coupled to one another by a mutual factor of ω_c. The electric susceptibility is obtained by taking the Fourier transform of the governing equations, solving the coupled linear system, and dividing the response of the driven oscillator in the fourier domain by the driving function.

$$\chi_1 = \frac{(\omega_{r;2}^2 - \omega^2 - i\beta_2\omega)}{(\omega_{r;1}^2 - \omega^2 - i\beta_1\omega)(\omega_{r;2}^2 - \omega^2 - i\beta_2\omega) - \omega_c^4} \quad \text{(II.2)}$$

Eq II.2 is the theoretical susceptibility corresponding to the linear dipole resonator in the coupled linear oscillator model. Immediately we see that the real part of the susceptibility vanishes at the split ring resonance frequency. This accounts for the PIO effect in the metamaterial. The prediction that the PIO resonance frequency is controlled by the split ring resonators is supported by experimental observation. From the derived bright mode susceptibility, we analytically obtain the transmission spectrum of the metamaterial.

$$T = \frac{(n-1)^2 + K^2}{(n+1)^2 + K^2} = \frac{(Re[\sqrt{1+\chi_1}] - 1)^2 + Im[\sqrt{1+\chi_1}]^2}{(Re[\sqrt{1+\chi_1}] + 1)^2 + Im[\sqrt{1+\chi_1}]^2} \quad \text{(II.3)}$$

The transmission spectrum (*Eq* II.3) is numerically fitted to the experimental spectrum. The treatment of confounding parameters in *Equation II.1* involved first visually plotting and identifying the prominent characterizing features of the transmission spectrum, namely frequency of the PIO interference, the width of the transmission curve, and the width of the PIO dip. The parameters that affect each of these features are then identified by manually adjusting one at a time. As we shall see in *Section III-1*, the resonance frequencies of the oscillator correspond to the location of the PIO resonance, the damping factors relate to the width of the transmission features, and the coupling frequency relates to the PIO strength and the broadening of the transmission decrease region. The procedure to resolve confounding variables is to first set the coupling strength ω_c to zero before increasing the dipole resonator damping rate to match the experimental transmission width. After an approximate damping rate for the dipole resonator is obtained, the coupling strength could be fitted while including small variations of the dipole damping rate.

II.2 Time Domain Response:

The plasmonic oscillator equations (II.1) were solved in the time domain numerically using a two-step euler method. THz-TDS data was supplied by the Y.S. Lee Group and imported for numerical analysis in python by reformatting into a numpy array. The TDS measurement sampling rate is at about 30 THz, meaning data points are separated by 1/30th of a picosecond. The *i*th index of this array is related to the time,

$$t = idt + t_{min} \text{ ,} \tag{II.4}$$

where *dt* is the time difference between data points and t_{min} is the beginning time of data collection relative to the peak THz field. This relation was used to translate *eq II.4* into equations relating elements in arrays,

$$q_1[i+1,j] = 2q_1[i,j] - q_1[i-1,j] - \beta_1(q_1[i,j] - q_1[i-1,j])dt - \omega_1^2 q_1[i,j]dt^2 \\ -\omega_c^2 q_2[i,j]dt^2 + QE_{inc}[i] \tag{II.5}$$

The first derivative term in *eq II.5* is asymmetric as a backward step derivative is used. To remedy this a second iteration of the oscillation array is computed, this time using the average of the forward and backward steps for the first derivative in the damping term,

$$q_1[i+1,j] = 2q_1[i,j] - q_1[i-1,j] - \frac{\beta_1}{2}(q_1[i+1,j] - q_1[i-1,j])dt - \omega_1^2 q_1[i,j]dt^2 \\ -\omega_c^2 q_2[i,j]dt^2 + QE_{inc}[i] \tag{II.6}$$

The fitting procedure laid out in *Section II.1* is capable of identifying all parameters in the above equation, with the exception of the coupling parameter *Q* to the incident field. The time domain response amplitude is directly proportional to this dipole coupling parameter. Once the response is solved for the solution can thus be scaled by the factor Q.

II.3 Mean Electron Velocity and Energy:

Photoexcitation of the intrinsic GaAs substrate generates mobile electrons. These mobile electrons then respond to the THz field following the optical pulse according to the Drude model[6,7],

$$v[i+1] = v[i] - \frac{e}{m} E_{THz}[i]dt - \frac{v[i]}{\tau_\Gamma} dt \quad . \tag{II.7}$$

The average kinetic energy of the electrons is calculated with the kinetic energy of the mean electron velocity added to the classical equipartition energy for a free gas.

$$u[i] = \frac{m_\Gamma}{2} v[i]^2 + \frac{3}{2} k_b T \tag{II.8}$$

The energy featured in *eq II.8* assumes a perfectly parabolic Γ - valley band structure. For low THz fields this is a decent approximation, however higher field strengths are able to transfer enough energy to push the electrons into non-parabolic regions. A first order correction for the non-parabolic Γ - valley electron energy is obtained by an energy dependant correction of the effective mass,

$$m_\Gamma \rightarrow (1 + 0.61U) m_\Gamma. \tag{II.9}$$

II.4. Intervalley Scattering Calculation

Sufficient electron energy is required to tunnel into side valleys. The Γ- L valley minimum energy difference, about 0.29 eV, would be required of photoelectrons for unassisted tunneling to occur into the L valley. Electron-phonon scattering however lowers the threshold energy for the intervalley transition to occur. We characterize the Γ- L intervalley scattering rate with a low energy range where no tunneling occurs, a high energy range where the tunneling rate is constant, and an intermediate energy range where the rate takes an intermediate value. In the model used here the intermediate intervalley transition rate occurs around a threshold energy E_{th}, with a width of this intermediate region ΔE_{th}.

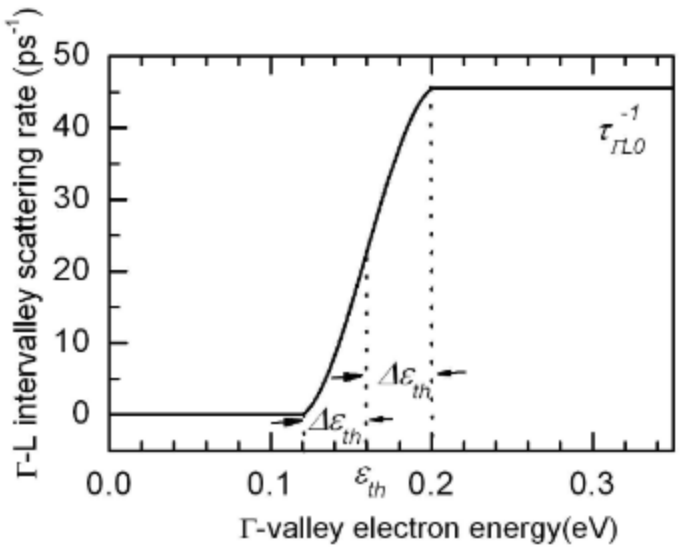

Figure II-2. Model Γ-L intervalley scattering rate with Γ valley electron energy. The three parameters used in this model are the minimum scattering time $\tau_{\Gamma L0}$, the threshold energy E_{th}, and the threshold energy width ΔE_{th}.

In the original model applied in the paper by Su, F. H., et al.[6] the behavior of the intervalley scattering rate function is an undisclosed 7th order polynomial that is continuous up to the third derivative at the edges of the threshold energy region. For simplicity our model used a cosine function in the intermediate energy region, which is chosen due to the continuity in all derivatives,

$$\tau_{\Gamma L}(\tau_{\Gamma L0}, E_{th}, \Delta E_{th})^{-1} = \frac{1}{2\tau_{\Gamma L0}}(1 - cos(\frac{\pi(u - (E_{th} - \Delta E_{th}))}{2\Delta E_{th}})). \quad \text{(II.10)}$$

A simple model is required since more rigorous calculations of phonon assisted intervalley scattering rates involve complicated matrix elements of deformation potentials[9]. We intend to capture the general behavior of this interacting system with the simpler model of *eq II.10*.

II.5. Determination of Scattering Rates

The scattering of electrons between states of higher and lower conductivity can be simplified by considering a two state system. The relative electron populations are governed by the relative sizes of the scattering times between the two states[7,10],

$$\frac{\partial n_\Gamma}{\partial t} = \frac{(n_{opt} - n_\Gamma)}{\tau_{L\Gamma}} - \frac{n_\Gamma}{\tau_{\Gamma L}} \,. \tag{II.11}$$

The relaxation time of side-valley electrons back down to the Γ-valley, given by $\tau_{L\Gamma}$ in equation II.11, is assumed to be independent of THz field strength. In the absence of strong THz fields the $\tau_{\Gamma L}$ scattering time is large enough to neglect the first term in *eq II.11*. This will result in an exponential Γ- valley population convergence to the initial population size. The characteristic recovery time in the Γ- valley population is used to determine the L to Γvalley scattering time.

The L to Γ- valley recovery time is exhibited in the conductivity behavior, as $\sigma = en_\Gamma\mu$. At THz frequencies the field is varying slowly enough for the real part of the conductivity to dominate, or at least remain roughly constant in the frequencies being considered,

$$\sigma = \frac{Y_0}{d}(2 - (1+N)\frac{E_{tns}}{E_{inc}}) \,. \tag{II.12}$$

Equation II.12 allows for the extraction of the real conductivity from the ratio of the experimental transmitted and incident field. More specifically, the THz transmitted field without the presence of the optical pump is used for the incident electric field. The optically excited transmission exponentially approaches the unexcited transmission with a time $\tau_{L\Gamma}$ after intervalley scattering, since conductivity is proportional to the Γ valley electron population.

II.6. Substrate Damping:

In Section I.2 we introduced the idea that a conductive substrate leads to additional damping of the metamaterial resonators. The increased damping rate is assumed to be directly proportional to the substrate conductivity, which has been observed experimentally for individual resonators[4,5,6]. The procedure of Section II.1 is repeated using the transmission spectrum of an optically pumped sample. For convenience the resulting damping rate is reported *per charge carrier*.

Once the Γ valley population is obtained, the time domain response (section II.2) is solved again, but with the extra damping factor:

$$\begin{aligned} \beta_1 &\rightarrow \beta_1 + \beta_{substrate} n_{opt} \\ \beta_2 &\rightarrow \beta_2 + \beta_{substrate} n_{opt}, \end{aligned} \tag{II.13}$$

where $\beta_{\text{substrate}}$ is the damping factor introduced by each optically excited electron. The substrate damping factor is obtained by the same procedure laid out in *section II.1*, by fitting now to the experimental optically excited sample transmission frequency spectrum.

III. Results

III. 1. Application to Intrinsic Plasmonic Oscillations

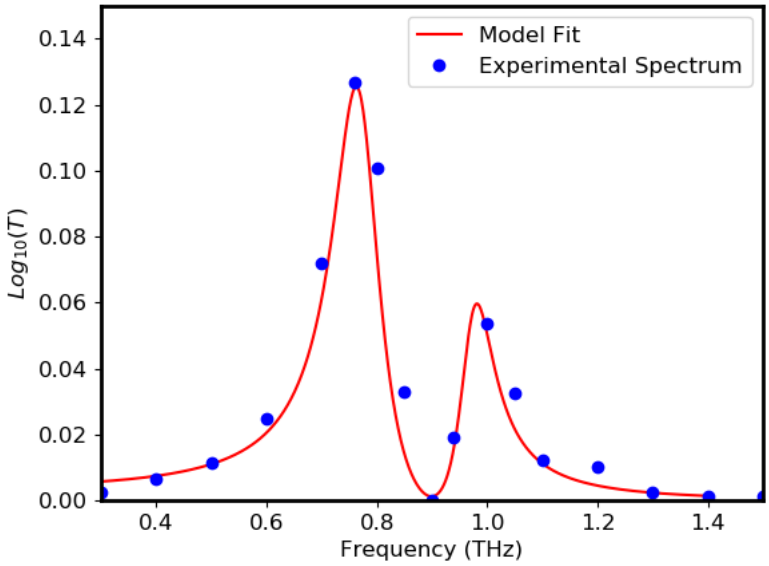

Figure III-1. Metamaterial transmission spectrum. In *red* the analytical result for the transmittance spectrum. In *blue* the experimental transmittance spectrum.

The parameters of the governing differential equation (*Equation II.1*) are required to solve for the field oscillation in an experimental setup. Extremal features of the experimental transmittance spectrum, shown in blue in *Figure III-1*, are used to estimate constraints on the numerical fitting range in parameter space. The first and most obvious feature of the spectrum is the location of the maximum PIO interference at 0.9 THz. The real part of the dipole resonator susceptibility (*equation II.2*) vanishes at the SSR resonance frequency ω_2. This vanishing of the susceptibility results in a minimization of the transmission (*Eq II.3*). The PIO interference is then a direct measurement of the dark mode resonance frequency ω_2. The bright mode resonance frequency must be somewhat close to the dark mode resonance for the PIO effect to take place, as was depicted qualitatively in *Figure I-2*. We expect that an exact matching of the two resonances at 0.9 THz would produce a symmetric transmission spectrum, however the experimental transmission is skewed slightly toward lower frequencies. From this shift we estimate the bright mode resonance to occur at 0.85 THz.

The width of the transmission spectrum without the PIO dip indicates that the damping rate in the bright mode resonator is about $\beta_1 \approx$ 0.2 (2π) ps^{-1}. Coupling strength and the dark mode damping rate both broaden the PIO frequency range. To parse these confounding parameters, the limit of little dark mode damping rate β_2 is used for fitting the coupling strength, which came out to about $\omega_c \approx 0.4\ (2\pi)\ ps^{-1}$. The final fit for the parameters of *Equation II.1* have $\omega_1 = 0.85\ (2\pi)\ ps^{-1}$, $\omega_2 = 0.9\ (2\pi)\ ps^{-1}$, $\beta_1 = 0.15\ (2\pi)\ ps^{-1}$, $\beta_2 = 0.05\ (2\pi)\ ps^{-1}$, and $\omega_c = 0.42\ (2\pi)\ ps^{-1}$.

The parameters fitted from the transmittance spectrum fully determine the differential equations of the metamaterial plasmon oscillations. These parameters allow for the step procedure outlined in *Section II.2* to be performed to get the time domain response. *Figure III-3* demonstrates the replication of the experimental THz field transmission by the linear oscillator model without the presence of the optical pump. The dipole coupling strength Q in *Equation II.1* simply scales the electric field response amplitude from the optically unexcited sample. To match the amplitude of the response to experiments, the coupling constant is set to $Q = 2 \times 10^{-3}$.

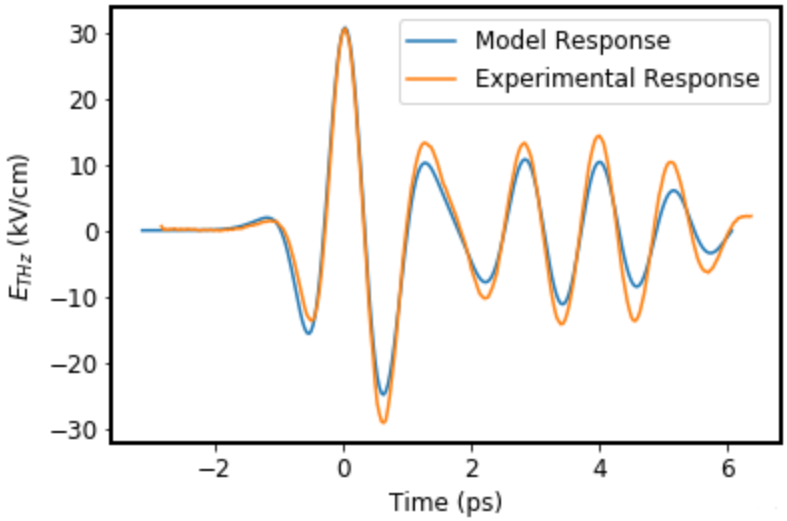

Figure III-3. Time response to incident THz wave without optical pulse. Response determined by euler step algorithm with time steps at 1/30th sec. The diff eq solutions are shifted back 8/30th of a second to fit over the metamaterial response.

Optical excitation of the sample resulted in a sudden rise in the substrate conductivity, which was hypothesized to correspondingly increase the damping on both resonators. After testing many possible substrate damping rates, an increase of 0.5 (2π) THz for about 10^{26} charge carriers injected by an optical pump fluence of 110 μJ/cm^2 best reproduce what is seen in the experimental setting. *Figure III-4* demonstrates the replication of the experimental optically excited substrate-metamaterial response.

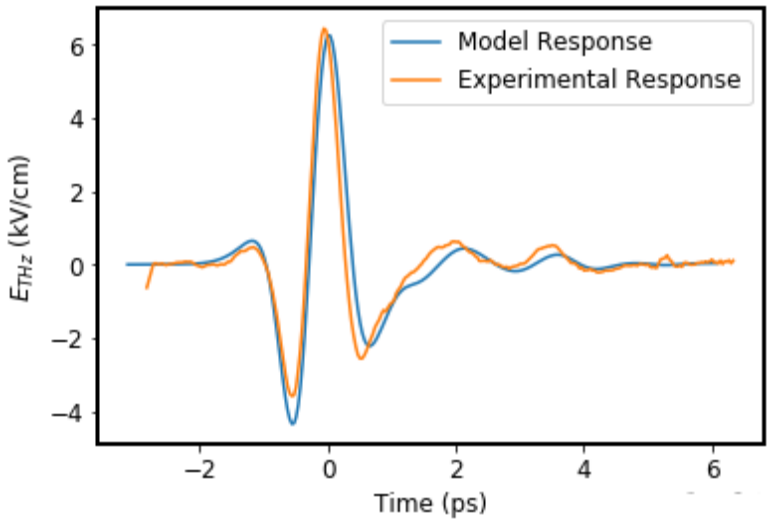

Figure III-4. Time response to incident THz wave with optical pulse. The metamaterial resonator damping rates are increased to 0.5 (2π) THz.

The increasing of the substrate conductivity inhibited the dipole coupling factor Q by a factor of 2.

III. 2. GaAs Substrate Conductivity

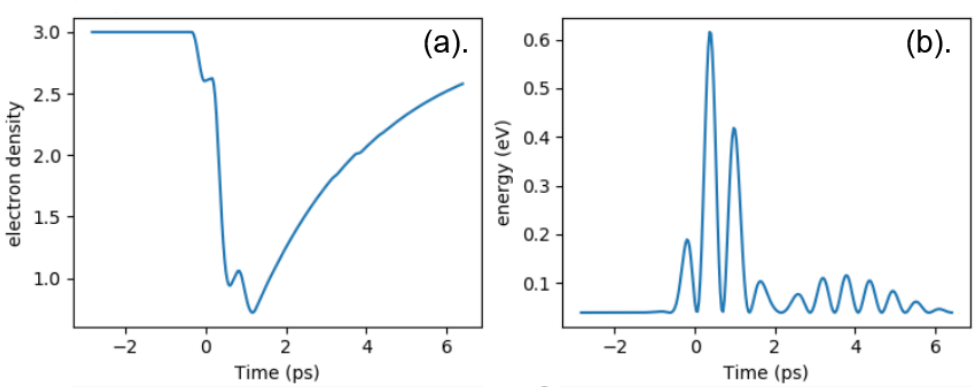

Figure III-5. (a). Γ-valley electron population after THz absorption. (b). Γ-valley electron mean kinetic energy.

The modelling of the intervalley scattering of conduction electrons in the GaAs involves a 2-state population model described in *Section II.6.* The time evolution of the valley populations is defined by the intervalley scattering rates $\tau_{L\Gamma}$ and $\tau_{\Gamma L}$ featured in *Equation II.11*. The $\tau_{\Gamma L}$ scattering rate however is controlled by the mean kinetic energy of Γ-valley electrons, which is solved for using *Equation II.7* and *II.8*. *Figure III-3*,(b) captures the mean electron kinetic energy transferred from the applied THz field. This mean electron kinetic energy brings the Γ-valley electrons into a region of their band structure where tunneling occurs at a rate determined by *E*quation II.10.

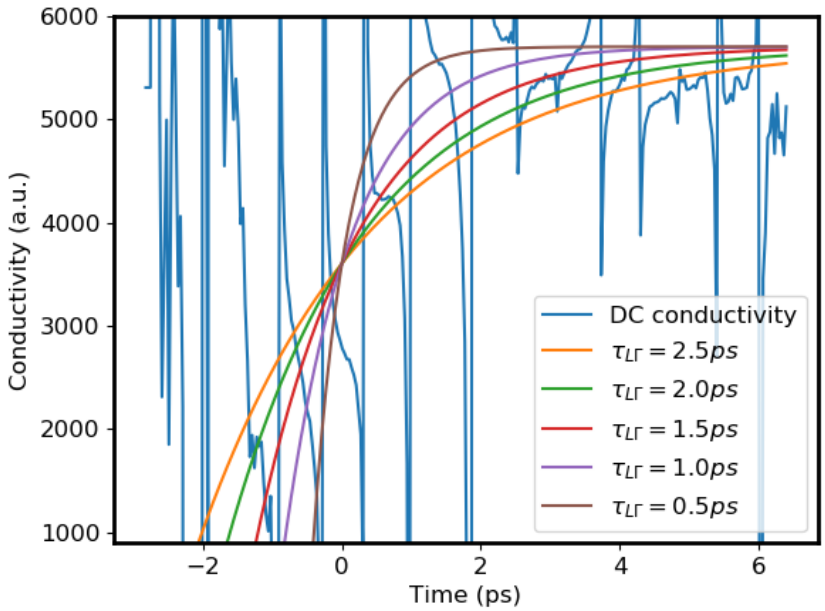

Figure III-6. (Blue) Experimental slow field DC conductivity as a function of time from eq (II-). Time (ps) is on the horizontal axis and conductivity ($\Omega^{-1}s^{-1}$) on the vertical axis. Other lines are exponential functions of the form $A(1 - e^{-t/\tau})$with characteristic times 0.5 ps, 1.0 ps, 1.5 ps, 2.0 ps, and 2.5 ps.

The intervalley relaxation rate $\tau_{L\Gamma}$ from the higher energy L-valley state back down to the lower energy Γ-valley state is obtained by taking the ratio of the transmitted and incident electric fields from the THz-TDS measurements provided by the Lee Lab, as indicated by *Equation II.12*. *Figure III-6* shows this experimental ratio, in blue, compared with several exponential trendlines with different characteristic times. A relaxation time of $\tau_{L\Gamma}$ = 1.5 $\pm$ 0.5 ps is the value used for subsequent calculations in the model.

The maximum intervalley excitation rate $\tau_{\Gamma L0}$ is more difficult to deduce since there's also a dependence on the threshold energy and energy width in *Equation II.10.* An estimate of $\tau_{\Gamma L0}$ = 0.035 $\pm$ 0.015 ps is made based on experimental luminescence[11] and optical pump-probe[12] spectroscopies, as well from theoretical results[6].

III. 3. Resonance Control

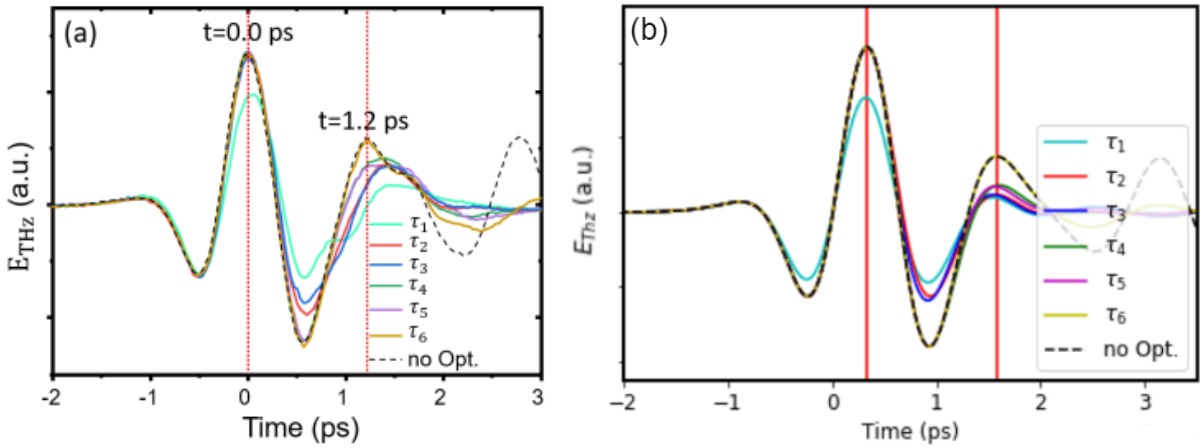

Figure III-7. (a) Experimental damping of transmitted THz field at optical pump delay times $\tau_{1-6} = -0.07, 0.37, 0.53, 1.00, 1.17, 1.93\ ps$.(b). Computational reproduction of the optical damping at the same delay times.

THz transmission is low following optical excitation. For longer optical pulse delays the full plasmon oscillations assist transmission. For overlapping optical and THz pulses several modulations in the differential transmittance are experimentally observed with varying delay times. Differential transmittance strongly varies with THz field strength. Neither the transmission modulations nor the field strength dependence are fully accounted for in a single valley model for the substrate conductivity.

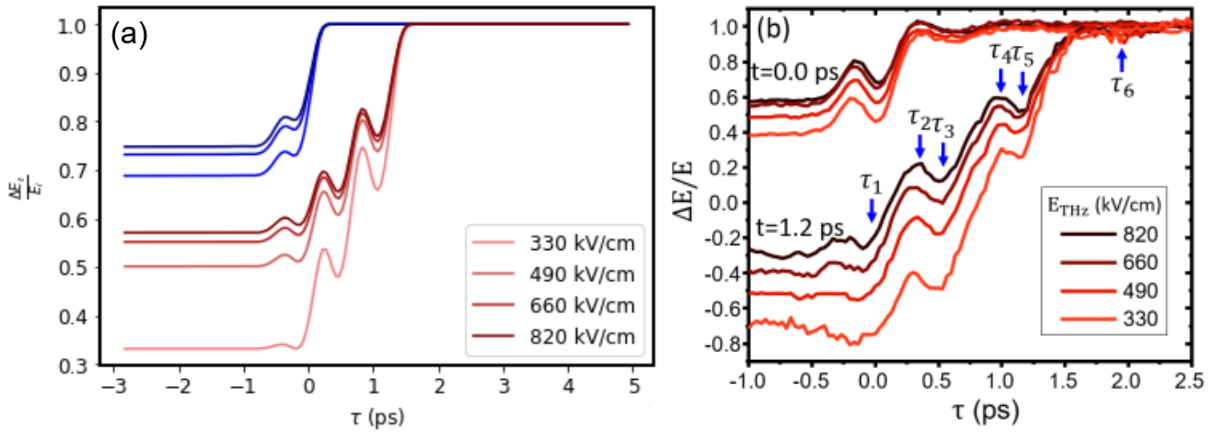

Figure III-8. Transmission of optically excited metamaterial relative to unexcited response. Relative transmission at t = 0.0 ps (top curves) and t = 1.2 ps (bottom curves). (a). Computational relative transmission without inclusion of intervalley scattering. (b). Experimental[2] transmission with arrows indicating τ_{1-6} = -0.07, 0.37, 0.53, 1.00, 1.17, 1.93 ps.

Figure III.8 shows the differential relative transmission of the THz pulse for different optical delay times. Generally the differential transmission is lower when the optical pulse precedes the THz pulse. There are however several modulations in the transmission which can be accounted for by the pulse shape of the THz field. The dependence of the differential transmission on THz field strength implicates a control over the metamaterial damping. This damping is directly manipulated by the THz pulse, which is seen as the damping control is lost after τ_5 = 1.17 ps.

IV. Discussion

IV. I. Physics of Plasmon Induced Opacity

Metamaterial plasmonic oscillations observed by THz-TDS measurements are well described by a coupled linear oscillator model. The resonance frequency of the dark mode split ring resonator determines the frequency of the maximum PIO effect. Since the incident THz field only strongly couples to the linear dipole resonator, the opacity is assumed to be caused by energy storage and dissipation in the SRR pair[13]. Here an analogy can be made with Newton's cradle, where energy is transferred through intermediate objects in contact with one another. The incident THz field first induces plasmonic oscillations in the dipole resonator, then those currents inductively and capacitively induce plasmonic oscillations in the SRR pair. At the resonance frequency of the SRRs this plasmonic oscillation can be sustained, resulting in electromagnetic energy transfer. This is the source of the opacity at the SRR resonance frequency.

The susceptibility (*Equation II.2*) only exhibits the PIO interference when the SRR pairs have a low damping factor relative to the dipole resonator damping. The result of the lower intrinsic damping is that the PIO resonance essentially stores electromagnetic energy for short periods of time in the lightly damped SRRs, which allows the transmitted THz field to persist for several ps longer than the incident pulse. As the incident THz pulse passes through the metamaterial, the 0.9 THz frequency component of the field is transferred into the SRR plasmonic oscillations, which are invisible to the transmission spectrum in *Figure III-1.*, only for those frequencies to reappear at a later time (2 - 6 ps after the incident THz pulse).

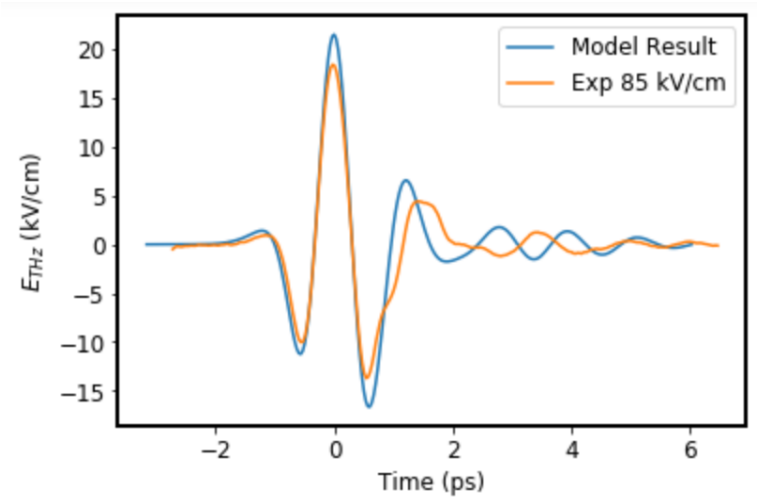

Figure IV-1. Comparison of model time-domain response with experimental THz-TDS for 12μJ/cm^2 optical pump fluence and 85 kV/cm THz field strength. Two unaccounted for phase shifts at approximately 0.8 ps and 1.7 ps are observed.

There are several discrepancies between our model's prediction and observed experimental THz-TDS response, particularly at lower optical pump fluences. The model fails to account for two phase shifts seen at approximately 0.8 ps and 1.7 ps in Figure *IV-1.* A phase shift at 1.7 ps has been present in all of the model results presented in this thesis and can be attributed to the "ringing" of the plasmon resonance with time, however the actual size of the phase shift could be underestimated. The plasmonic oscillation is likely "pushed back" while the high THz field is still present, which would increase the size of the phase shift.

IV. 2. Decreased Damping by Intervalley Scattering

THz control of the damping of the metamaterial oscillations is governed by electron scattering rates between high and low conductivity states. These differing conductivity states are offered by different valleys in the GaAs conduction band structure. A higher scattering rate from the more conductive Γ-valley to the less conductive *L* and *X*-valleys corresponds to an increased sensitivity of the metamaterial-substrate plasmonic damping to THz field strength._
The results presented in *Figure III-6.* are particularly useful for understanding the effects of intervalley scattering on the system. When the incident THz pulse arrives long before the optical pulse, the metamaterial responds without much damping. This is seen in the figure for sufficiently large optical-THz delay times ($\tau > 1.5$ ps), where the transmitted field is equal to the response from the unexcited sample. Intervalley scattering of Γ-valley electrons can only occur in a photoexcited sample, and the strength of the THz field after photoexcitation decreases the damping of the metamaterial response. Going from $\tau = 1.5$ ps to $\tau = 0$ ps has the optical pulse preceding an increasing amount of the THz pulse duration, which explains the progressive splitting of the lines in this overlap region. The moving back of the optical pulse relative to the THz allows for more of the THz to induce intervalley scattering. One of the most striking features of *Figure III-6* are the several modulations in the damping at the $\tau_{1\text{-}6}$ delay times. The modification of the metamaterial resonance frequencies shifts these modulation times, indicating that plasmonic oscillations of the metamaterial are themselves inducing intervalley scattering in the photo excited substrate. Additionally, decreasing the damping rate of the plasmonic oscillations dramatically increases the size of these modulations.

The divergence of the several line plots of *Figure III-6* are controlled by the rate of intervalley tunneling. The number of electrons occupying the less conductive side bands at any moment is governed by the *ratio* of the excitation and relaxation scattering times, as can be seen in the equilibrium solutions to *Equation II.11.* Running our simulation after increasing the intervalley excitation time from 35 fs, to 500 fs, and then up to 1 ps, we are able to observe the changes to *Figure III-8* as shown in *Figure IV-2*.

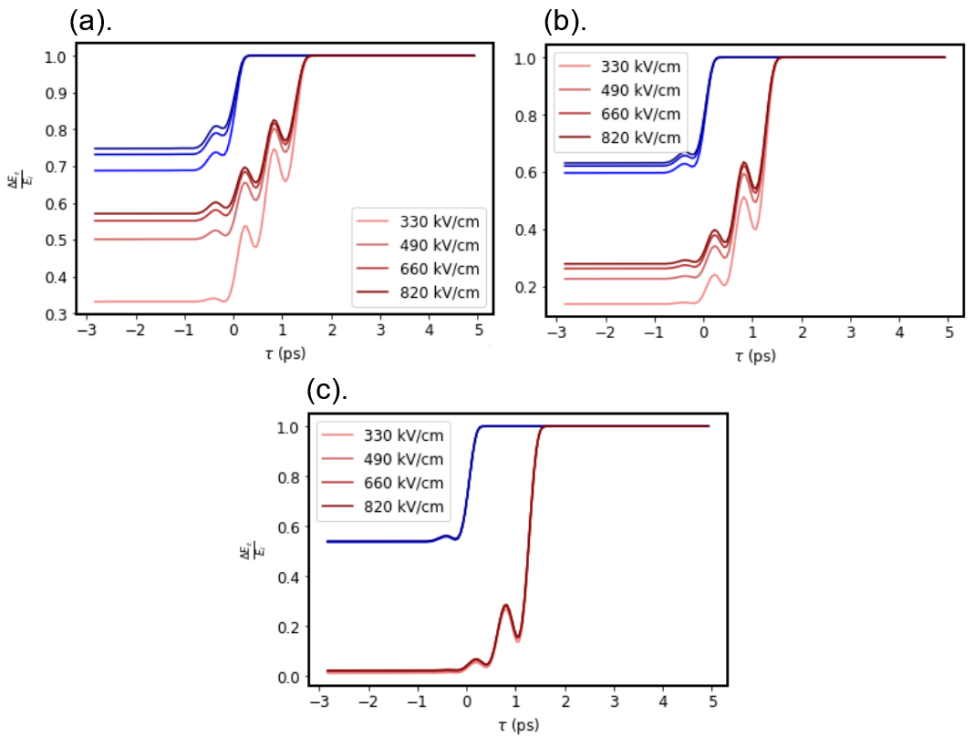

Figure IV-2. Effect of increasing the intervalley excitation time $\tau_{I\Gamma L}$ relative to intervalley relaxation rate. The differential transmission plot with optical delay time for $\tau_{I\Gamma L}$ = 35 fs (a), 500 fs (b), and 1 ps (c).

Our model shows the dependence of differential transmission on THz field strength to be strongly dependent on intervalley scattering rates within the semiconductor substrate. Optical pulse THz transmission experiments using different THz field strengths can be related to a numerical calculation to find information regarding intervalley scattering rates in the sample, which can provide insights into the electronic band structure and/or many body scattering effects.

IV. 3. Replication of Experiments

The purpose of the computational model developed here is to demonstrate that increased conductivity in the metamaterial substrate induces damping in plasmonic oscillations. *Figure 5* shows the replication of the damping behavior in low THz fields for different optical delay times. Here the substrate is assumed to have an equal damping effect on both the radiant and subradiant structures. No change in the coupling frequency between the metamaterial resonators is accounted for in this model, which appears to be unimportant for the qualitative replication of these experimental results.

The altering of the metamaterial plasmonic damping by strong THz fields are attributed in this model to induced scattering of electrons between high and low conductivity states in the substrate.

The relative transmission restoration is attributed to the conductivity drop associated with gamma-valley population decrease. The magnitude of the restoration is determined by the intervalley scattering time ratio. The response to the overlapping optical-THz pulses is replicated by the particular values of the scattering rates.

V. Summary and Conclusion

The plasmon-induced opacity signature in the optically-unexited metamaterial is observed in the coupled linear oscillator model in the case when the driven oscillator, or "bright mode" experiences high damping. The disappearance of the PIO effect after optical excitation and subsequent reintroduction by strong THz fields is described by allowing time dependent damping to the system. With an additional time-dependent damping term added to both oscillators in proportion to substrate conductivity, I'm able to replicate the THz response of the metamaterial seen by THz time domain spectroscopy measurement. Perhaps the most interesting feature of the time-dependent damped oscillator model is the prediction that sufficiently strong plasmonic oscillations in a metamaterial can itself drive transitions between different valleys in the band structure of the substrate material. This prediction was observed in experimental transmission over different optical-THz pulse delay times, providing a quantitative interpretation. The simple and controllable oscillations in a well designed metamaterial provide a convenient probe of substrate electronic states by observing small modulations in the differential transmission of THz waves.

The time-independent parameters of the coupled oscillator model were found by first deriving the transmission by taking the Fourier transform of the coupled oscillator differential equations and solving the system. This derived transmission is fitted to Fourier transformed THz-TDS measurements of the metamaterial described in *Figure I-1*. These oscillator model parameters for the example system are then used to derive the time domain response is successfully derived by means of numerical integration.

Optical and THz pulses introduce additional time dependence to the metamaterial system, particularly in the substrate conductivity. The inclusion of substrate conductivity time variation is accounted for by allowing time dependence in the oscillator damping rates. We assumed that the increased oscillator damping rates were directly proportional to substrate conductivity. The substrate conductivity is then modelled as a two-state system with the population dynamics intended to capture the intervalley tunneling of electrons from the conductive Γ valley to less conductive side valleys. These tunneling rates were based on the simplified model employed by Su, F. H., et al. with parameters estimated based on a

combination of previous works and the observed recovery time of experimental substrate conductivity by the Lee Lab. After finding good numbers for the Su, et al. intervalley model parameters, the time-domain THz response after optical excitation of the GaAs substrate is solved with our theoretical model and subsequently compared with experiment. We find that the coupled oscillator model qualitatively replicates the THz response behavior seen in experiments. The magnitude of the optical damping for different THz field strengths however could not be obtained while simultaneously replicating the details of the plasmonic oscillation behavior in time.

Despite the apparent limitations of the coupled oscillator model, its simplicity and generality allows for a first-order model of a wide range of plasmonic metamaterials. Interesting pertinent features of experimental THz responses, such as the location of phase shifts or the transmission modulations of *Figure III-8*, are expected to vary with the metamaterial properties as depicted in our oscillator model. Along with different metamaterial designs, our model is also capable of producing the THz response to arbitrary incident pulse shapes. This is the versatility of the coupled linear oscillator model. This work has demonstrated the influence of optical and THz fields are accounted for by allowing oscillator damping to vary in proportion to substrate conductivity, expanding applicability to more complex metamaterial-light interactions.

VI. Acknowledgements

Working toward this project has been invaluable for keeping my life right-side up during the COVID-19 quarantine. I'd like to thank Dr. Yun-Shik Lee for providing me this opportunity and for keeping me busy. His guidance has allowed this project to proceed smoothly and productively. I also thank Alden Bradley for attending my meetings and clearing up misconceptions of mine. Both Dr. Lee and Alden gave much needed writing feedback as well, especially with more technical aspects of the thesis.

I thank Professor Janet Tate, Dublin Nichols, and my classmates in Physics 403 for their advice and inspiration in writing the bulk of this thesis. I feel the final product is as much their input as it is my own work.

VII. References

[1]. Sirtori, C. Bridge for the terahertz gap. *Nature* **417,** 132–133 (2002). https://doi.org/10.1038/417132b

[2]. Mousavian, A., Thompson, Z. J., Lee, B., Bradley, A. N., Sprague, M. X., & Lee, Y. S. (2021). Strong-field terahertz control of plasmon induced opacity in photoexcited metamaterial. *JOSA B*, *38*(4), 1163-1166.

[3]. Jackson, John David. "Classical electrodynamics." (1999): 841-842.

[4]. Kim, T. T., Kim, H. D., Zhao, R., Oh, S. S., Ha, T., Chung, D. S., ... & Zhang, S. (2018). Electrically tunable slow light using graphene metamaterials. *Acs Photonics*, *5*(5), 1800-1807.

[5]. He, X., Wang, Y., Tao, M., Yu, X., Pei, Z., Wang, B., ... & Geng, Z. (2019). Dynamical switching of electromagnetically induced reflectance in complementary terahertz metamaterials. *Optics Communications*, *448*, 98-103.

[6]. Su, F. H., Blanchard, F., Sharma, G., Razzari, L., Ayesheshim, A., Cocker, T. L., ... & Hegmann, F. A. (2009). Terahertz pulse induced intervalley scattering in photoexcited GaAs. *Optics express*, *17*(12), 9620-9629.

[7]. Tassin, P., Zhang, L., Koschny, T., Economou, E. N., & Soukoulis, C. M. (2009). Low-loss

metamaterials based on classical electromagnetically induced transparency. *Physical review letters*, *102*(5), 053901.

[8]. Kuehn, W., Gaal, P., Reimann, K., Woerner, M., Elsaesser, T., & Hey, R. (2010). Terahertz-induced interband tunneling of electrons in GaAs. *Physical Review B*, *82*(7), 075204.

[12]. Liu, X., Gu, J., Singh, R., Ma, Y., Zhu, J., Tian, Z., ... & Zhang, W. (2012).

[9]. Zollner, S., Gopalan, S., & Cardona, M. (1990). Microscopic theory of intervalley scattering in GaAs: k dependence of deformation potentials and scattering rates. Journal of applied physics, 68(4), 1682-1693.

[10]. Stanton, C. J., and D. W. Bailey. "Rate equations for the study of femtosecond intervalley scattering in compound semiconductors." *Physical Review B* 45.15 (1992): 8369.

[11]. Shah, J., Deveaud, B., Damen, T. C., Tsang, W. T., Gossard, A. C., & Lugli, P. (1987). Determination of intervalley scattering rates in GaAs by subpicosecond luminescence spectroscopy. *Physical review letters*, *59*(19), 2222.

[12]. Becker, P. C., Fragnito, H. L., Brito Cruz, C. H., Shah, J., Fork, R. L., Cunningham, J. E., ... & Shank, C. V. (1988). Femtosecond intervalley scattering in GaAs. *Applied physics letters*, *53*(21), 2089-2090.

[13]. Liu, X., Gu, J., Singh, R., Ma, Y., Zhu, J., Tian, Z., ... & Zhang, W. (2012). Electromagnetically induced transparency in terahertz plasmonic metamaterials via dual excitation pathways of the dark mode. *Applied Physics Letters*, *100*(13), 131101.